

leading to homogeneous formation of CO_x . Support for the importance of the homogeneous process consists of calculations which show that the rates of the competing reactions are comparable to the coupling reaction of CH_3 to form C_2H_6 , and the detection of increased concentrations of C_3H_6 when $^{13}\text{C}_2\text{H}_4$ is added to the CH_4/O_2 mixture.

(iii) Results for the ^{13}C content of CO and CO_2 , though scattered, are consistent with CO oxidation being the source of the CO_2 .

(iv) There is an exchangeable pool of CO_2 on the catalyst which

is indicative of the presence of Li_2CO_3 under reaction conditions.

Acknowledgment. We thank R. J. Tyler for his enthusiastic encouragement of this work, and C. A. Lukey for some calculations of conversion and selectivities. This project was supported by the Macquarie University/CSIRO Collaborative Fund and a NERDDP grant to the Broken Hill Proprietary Company, Melbourne Research Laboratories.

Registry No. CH_4 , 74-82-8; CO , 630-08-0; CO_2 , 124-38-9; Li , 7439-93-2; MgO , 1309-48-4; C_2H_6 , 74-84-0; C_2H_4 , 74-85-1.

Scanning Tunneling Microscopy and Tunneling Spectroscopy of the n-TiO₂(001) Surface

Fu-Ren F. Fan and Allen J. Bard*

Department of Chemistry, The University of Texas at Austin, Austin, Texas 78712
(Received: September 18, 1989; In Final Form: February 6, 1990)

The (001) surface of a highly doped ($\sim 10^{19} \text{ cm}^{-3}$) n-type TiO_2 crystal, following polishing, wet etching, and cleaning, was imaged in air with a Pt-Ir tip with a scanning tunneling microscope (STM). Good images of the surface could be obtained with the sample held at negative voltage (positive tip bias), with the high-resolution image showing only Ti atoms. Tunneling spectroscopy, involving the recording of i - V curves and dynamic conductance (di/dV)- V curves with the tip held over a given spot on the TiO_2 surface, was also carried out. The resulting curves show electron tunneling into the conduction band and from the valence band, as well as a prominent peak identified as a surface state about 0.3 eV below the conduction band edge.

Introduction

This paper deals with a new approach to the study of the TiO_2 surface to obtain structural and energetic information. Transition-metal oxides and chalcogenides are known to be catalytically active for a large number of thermal and photoinduced chemical processes. Following the initial report on the application of TiO_2 in the photolysis of water,¹ numerous reports on the application of TiO_2 electrodes and particles as useful materials for the photooxidation of organic and inorganic species have appeared.² From the earliest studies of chemical photoprocesses at TiO_2 ,^{2d} it became clear that the surface energetics and surface states play an important role in the efficiency and range of applicability of this, and other, semiconductor materials. Theoretical calculations of surface electronic structure and experiments using surface-sensitive electron spectroscopic techniques (e.g., low-energy electron diffraction (LEED) and ultraviolet photoemission spectroscopy (UPS)) have been performed on various surfaces of this material. While progress has been made in understanding certain specific surface structures and defects, and chemisorption systems,³ observations on the atomic or near-atomic scale of the surface and its geometric defects and chemical adsorbates have hitherto not been possible. While information about surface energetics and surface states can be obtained by UHV techniques like UPS and inverse photoemission spectroscopy (IPS), there remains a need for complementary methods, especially ones that can be used with the sample under conditions of its use as a catalyst or electrode, e.g., exposed to gases or liquids.

Following the introduction of the scanning tunneling microscope (STM) by Binnig and Rohrer,⁴ a number of studies have ap-

peared on the use of the STM to produce high-resolution topographic images and to provide electronic structural information about surfaces of semiconductors and metals, as well as adsorbate-covered surfaces.⁵ Studies of samples immersed in liquids and used as electrodes have also appeared. For example, there have recently been two communications concerning studies of TiO_2 with the STM.^{6,7} Gilbert and Kennedy⁶ imaged TiO_2 in air and investigated the effect of surface treatment (polishing, etching) on topography. Itaya and Tomita⁷ studied the TiO_2 /aqueous solution interface and the effect of substrate potential on the STM behavior. They found that good images could be obtained only when the n-type TiO_2 was held at potentials negative of the flat-band potential (i.e., with a TiO_2 accumulation layer at the interface). We report in this work the application of the STM and related spectroscopic techniques to the study of an n-type $\text{TiO}_2(001)$ surface in air and to the determination of surface electronic structures under these conditions.

Experimental Section

The (001) oriented n- TiO_2 single-crystal samples (Fuji Titan., ca. $5 \times 5 \times 1 \text{ mm}^3$) were mechanically polished to an optical finish by use of various grades of diamond and alumina polishing pastes ending with 0.05- μm alumina. The samples were then etched in molten KHSO_4 at 620 °C for 30 min⁸ and then boiled in a mixture of HNO_3 (45% vol), HCl (45% vol) and HF (10% vol) for 1 h⁹ to remove the residue from the chemical etch. The samples were next thoroughly rinsed with Millipore reagent water. After drying, the samples were reduced to a bluish-gray color (indicating a ca. 10^{19} cm^{-3} doping density) by heating in H_2 at 800 °C for ca. 30

(1) Fujishima, A.; Honda, K. *Bull. Chem. Soc. Jpn.* **1971**, *44*, 1148.
(2) (a) *Semiconductor Electrodes*; Finklea, H. O., Ed.; Elsevier: Amsterdam, 1988. (b) Bard, A. J. *Science* **1980**, *207*, 139. (c) Frank, S. N.; Bard, A. J. *J. Am. Chem. Soc.* **1977**, *99*, 303. (d) *Ibid.* **1975**, *97*, 7427.
(3) See, e.g.; Henrich, V. E. *Appl. Surf. Sci.* **1979**, *9*, 143, and references therein.
(4) Binnig, G.; Rohrer, H. *Helv. Phys. Acta* **1982**, *55*, 726.

(5) See, e.g.; (a) Quate, C. F. *Phys. Today* **1986**, *Aug*, 26. (b) Hansma, P. K.; Tersoff, J. *J. Appl. Phys.* **1987**, *61*, R1. (c) Kuk, Y.; Silverman, P. J. *Rev. Sci. Instrum.* **1989**, *60*, 165.
(6) Gilbert, S. E.; Kennedy, J. H. *J. Electrochem. Soc.* **1988**, *135*, 2385.
(7) Itaya, K.; Tomita, E. *Chem. Lett.* **1989**, 285.
(8) Fleishauer, P. D.; Chase, A. B. *J. Phys. Chem. Solids* **1974**, *35*, 1211.
(9) Johnson, O. W.; Park, S. H.; Deford, J. W. *J. Appl. Phys.* **1975**, *46*, 1026.

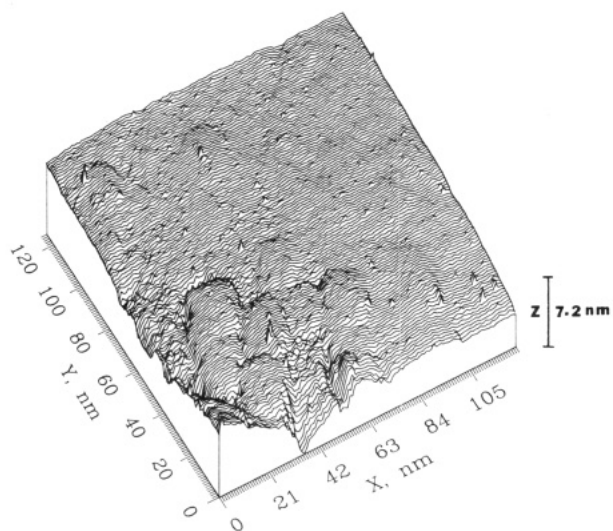


Figure 1. Typical unfiltered 128 nm \times 128 nm STM image of a polished, etched, and strongly reduced n-TiO₂(001) surface, acquired at a tip voltage of 1 V relative to the sample and a reference current of 0.5 nA. The rastering rate of the tip is ca. 2 lines/s. The total height range is ca. 73 Å.

min.¹⁰ A layer of In-Ga alloy was then plated on a small spot on the sample surface to serve as an Ohmic contact.

The STM used here utilized a micrometer-driven differential spring assembly for sample movement and a piezoelectric tripod to scan the tip.¹¹ The conductance spectra were obtained by triangularly sweeping the voltage (at ca. 2 V/s) between tip and sample while superimposing a small sinusoidal signal (modulation frequency 10 kHz) and recording the in-phase output on a lock-in amplifier operated at the modulation frequency.¹² The modulation voltage amplitude was ca. 10–20 mV peak to peak. A complete spectrum consisted of the average of about 10–50 scans collected over a period of a few minutes. Averaged spectra recorded at a single location on the sample were quite reproducible, when only data recorded on forward scans (i.e., from 0-V bias to either positive or negative bias) were used. In obtaining current vs voltage (i - V) or conductance vs voltage (di/dV vs V) curves, the distance between tip and substrate, s , (controlled by the z -piezo in response to changes in i) should be held constant. This was accomplished by gating the feedback control circuit to the z -piezo used for the constant-current mode operation of the STM so that it was active for 1 s between each scan. When the feedback loop was active, a constant voltage was applied to the sample; when inactive, the position of the tip was held stationary at the desired height and the tunneling current or conductance was measured as a function of bias voltage. The total length of a measurement cycle was a few seconds.

Electrochemically etched Ir-Pt (FHC Co., Brunswick, ME) tips were employed. The spectra reported here were obtained with relatively blunt tips. We believe that they represent a spatial average over at least a surface unit cell, because of the blunt tips and the small thermal drift (~ 1 Å/min) of the STM used here. We found that blunt tips were more stable and gave more reproducible spectra. Sharper tips were used for the STM images, however, and these produced larger corrugation amplitudes. All STM experiments were performed in air and in the dark.

Results and Discussion

STM Images. In Figure 1 we show a typical 128 nm \times 128 nm STM image of the n-TiO₂(001) surface acquired at a tip voltage of 1.0 V positive relative to the sample (henceforth referred to as the bias voltage) and a reference current of 0.5 nA. Our STM images at this resolution were similar to those of etched TiO₂ surfaces previously reported.^{6,7} The overall morphology of the

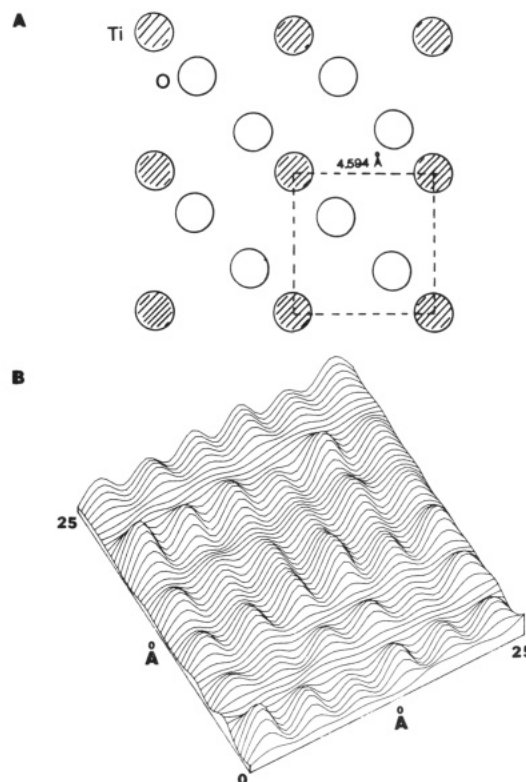


Figure 2. (A) Schematic view of the n-TiO₂(001) surface. Oxygen atoms are shown in white, and titanium atoms are shaded. A square surface unit cell is also shown. (B) A high-resolution current image obtained from an atomically flat region of the surface in Figure 1, acquired at the same voltage but with a reference current of 5 nA. The image is slightly filtered by a fast Fourier transform digital filter at a filter width of 0.1. The image extends laterally over an area of 25 \times 25 Å². The rastering rate of the tip was less than 2 lines/s. The current corrugation amplitude is in the range of 2.0–7.5 nA.

etched surface showed fairly large flat regions extending hundreds of angstroms laterally, coexisting with some depressions and a number of ditches. These defects could be caused by polishing and chemical etching or by surface reconstruction or facet formation under high-temperature annealing conditions, as suggested by Tait and Kasowski.¹³ In Figure 2A the structure of the ideal unrelaxed n-TiO₂(001) surface is shown. Each surface unit cell contains one titanium and two oxygen atoms, and successive layers differ only by a rotation of 90° from one another. In Figure 2B we show a higher resolution STM image obtained at a nearly atomically flat region. The atomic rows with nearly square surface structure are clearly seen; however, it is puzzling that both titanium and oxygen are not resolvable even at fairly positive bias voltages (e.g., >2 V), where electron tunneling from the valence band of n-TiO₂ to the tip might be expected to occur, as discussed below. The lattice constant for the square unit cell shown in Figure 2B is ca. 4.2 Å, compared to the accepted value of 4.594 Å.¹⁷ The difference between these values probably arises from a small calibration error (as referenced to highly ordered pyrolytic graphite). The peak-to-valley corrugation amplitude is in the range of 0.1–0.2 Å. We generally had to use a rather positive bias voltage (e.g., ≥ 1.0 V) to achieve the very stable tunneling current required for good STM imaging. We were unable to obtain stable STM images for either small positive or negative bias voltages, suggesting the lack of a sufficiently high density of low-lying gap states in the TiO₂ through which the current can pass. This is consistent with the results on conductance measurements which will be described later and the earlier STM studies of TiO₂.^{6,7}

STM Current-Voltage Spectroscopy Measurements. Two types of tunneling spectroscopic (TS) measurements were made with the tip held fixed at a given position above the TiO₂ surface.

(10) Cronmeyer, D. C. *Phys. Rev.* **1952**, *87*, 876.

(11) Fan, F.-R.; Bard, A. J. *Anal. Chem.* **1988**, *60*, 751.

(12) Fan, F.-R. F.; Bard, A. J. *J. Electrochem. Soc.* **1981**, *128*, 945.

(13) Tait, R. H.; Kasowski, R. V. *Phys. Rev. B* **1979**, *20*, 5178.

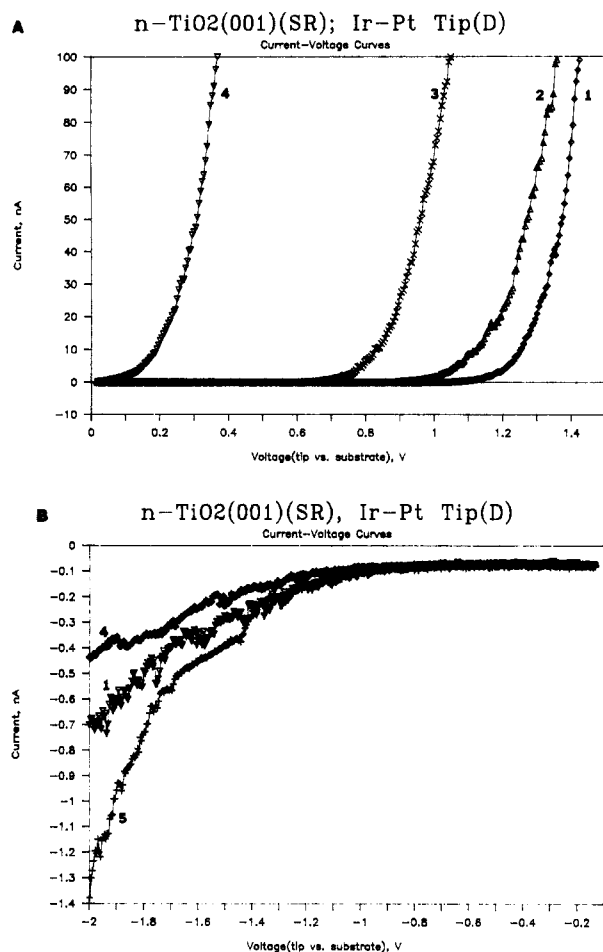
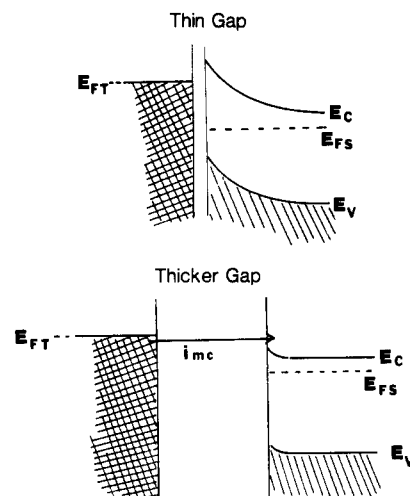


Figure 3. Current vs voltage ((A) tip positively biased and (B) tip negatively biased) curves for an Ir-Pt tip and n-TiO₂(001) sample at various tip-sample separations. 1, reference tip-sample separation (s_0) defined by a current 0.5 nA at bias voltage 1.0 V; 2, $s_0 - 5$ Å; 3, $s_0 - 10$ Å; 4, $s_0 - 20$ Å and 5, $s_0 + 20$ Å.

In i - V measurements the tip current was recorded as a function of tip bias (V). In conductance (di/dV) measurements the magnitude of the 10-kHz modulation current was determined as a function of V . The TS measurements reported here were taken at a small area of an atomically flat region. The curves obtained were reproducible for different locations within the flat region.

In Figure 3 the experimentally determined i - V relationships at various tip-sample separations, s , are shown. Since the absolute distance between tip and substrate cannot be obtained directly, we use the separation at a given current and voltage (e.g., $i = 0.5$ nA and $V = 1.0$ V, tip vs sample) as the reference gap (s_0). As shown, the i - V curves display strong rectifying behavior. For a given s , a much larger current is seen at positive bias compared to negative bias. For example, in curve 1 the current at +1.4 V is 78 nA whereas the current at -1.4 V is only -0.2 nA. It should be mentioned that the small current (ca. 0.06 nA) observed between 0 and -0.8 V is mainly contributed by the offset of our current-measuring amplifiers and perhaps also by the effect of a trace amount of room light. The magnitude of the current at a given positive bias was strongly dependent on s . The i - V behavior at a given s was nearly exponential. The presence of the insulating air gap provides an additional degree of freedom to the energy band diagram (see Scheme I), allowing the Fermi levels (and bands) of the tip and semiconductor surfaces to move energetically relative to one another. However, the insulating gap between the tip and the substrate cannot be thought of as a simple series impedance, since the distribution of potential between gap and semiconductor depends on the bias; this could affect the interfacial-charge-transfer kinetics dramatically. This might explain the rather peculiar results shown in Figure 3B, in which the reverse-bias current for a given bias less than -1.0 V increases

SCHEME I



with increasing s for the range of s studied. When the gap is very thin, since most voltage is absorbed by the semiconductor and very little voltage is developed across the gap, the tip Fermi energy cannot increase toward E_C . The increased transmission coefficient (κ) is overcompensated by the low concentration of electrons in the tip above the energy E_C . Thus, the resultant current is lower for thinner gap separation. However, when s is too large, the current drops again due to the decreased transmission coefficient. The magnitude of the reverse-bias current, as compared with the forward-bias i - V curves, is less dependent on s . Those behaviors are characteristic of a metal/insulator/semiconductor (MIS) tunneling junction.¹⁴ To obtain a more precise description, we have performed an independent series of experiments by measuring the current as a function of change in separation at various voltages. Typical curves at bias of 1 V are shown in Figure 4. Assuming that i behaves as⁵

$$i \propto \exp(-2\kappa s) \quad (1)$$

where κ is the inverse decay length of the tunneling current. κ is given by (2), where m is the electron mass and ϕ is the effective

$$\kappa = (2\pi/\hbar)(2m\phi)^{1/2} \quad (2)$$

barrier height. A value of 0.90 \AA^{-1} is obtained for κ , which gives an estimated effective barrier height for tunneling of ca. 3.2 eV. We have found that κ is almost independent of voltage at positive bias ($1 \text{ V} \leq V \leq 3 \text{ V}$). Because of the instability of the tunneling current at less positive and negative bias, we could not measure κ values reliably under these conditions by this technique.

We now move to the conductance measurement, which can provide electronic structural information, such as the energy band gap of semiconductors and the surface density of state (DOS) of the sample.⁵ We first describe the dynamic (or differential) conductance spectra (di/dV vs V) without normalizing with respect to the static (or integral) conductance (i/V). Figure 5 shows a typical conductance spectrum for a heavily doped (ca. $10^{19}/\text{cm}^3$) n-TiO₂(001) sample in the range from -2.8 to +3.3 V. Although the values of conductance were not normalized with respect to i/V , they were corrected for the dependence of i on s , by dividing the di/dV values by $e^{-2\kappa s}$. Note that there is a wide region of low conductance terminating at both ends in regions of rapidly rising conductance. This low-conductance region, referred to as the "conductance well", is close to the energy gap of the rutile form of TiO₂ (3.05 eV).¹⁷

In general, the observed tunneling current can be considered to be composed of components attributed to electrons tunneling

(14) Sze, S. M. *Physics of Semiconductor Devices*; Wiley: New York, 1981; Chapter 9.

(15) Tersoff, J.; Hamann, D. R. *Phys. Rev. Lett.* **1983**, *50*, 1998.

(16) Baratoff, A.; Binnig, G.; Fuchs, H.; Salvan, F.; Stoll, E. *Surf. Sci.* **1986**, *168*, 734.

(17) Grant, F. A. *Rev. Mod. Phys.* **1959**, *31*, 646.

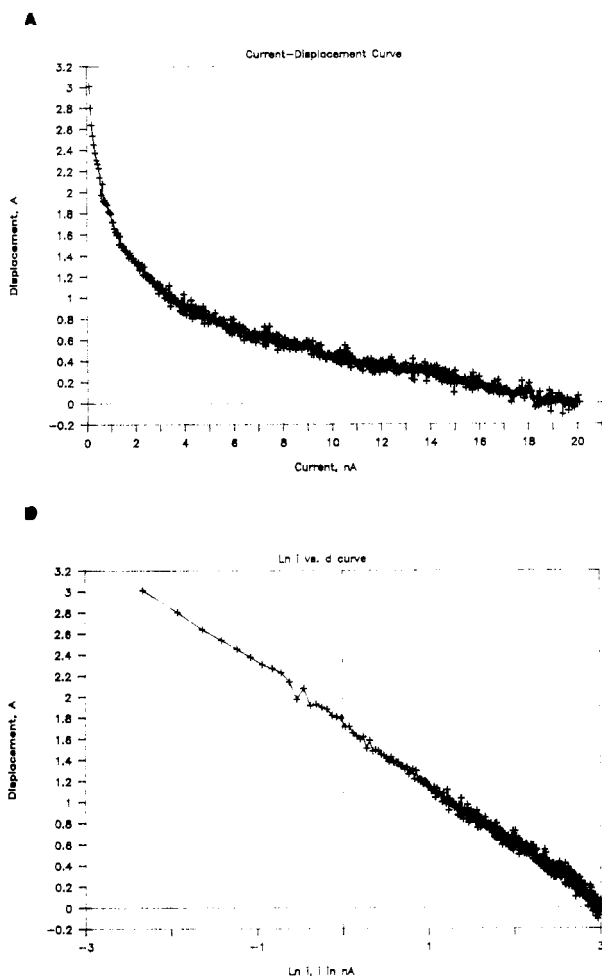


Figure 4. Current vs vertical tip displacement (A) and \ln (current) vs vertical tip displacement (B) at tip voltage of 1 V for an Ir-Pt tip and n-TiO₂(001) sample.

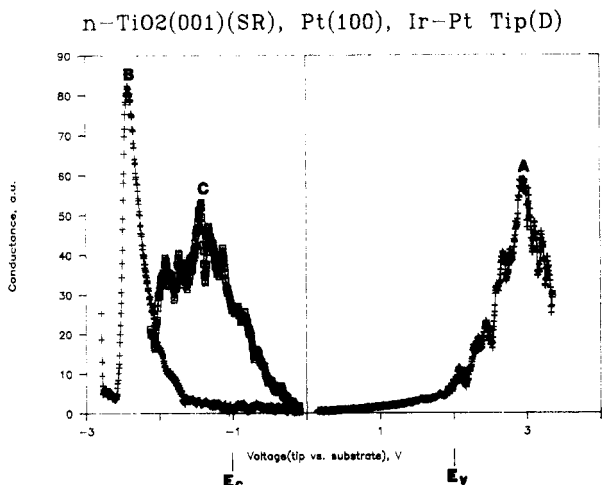


Figure 5. Dynamic (or differential) conductance (di/dV) as a function of tip voltage. Curves A and B are for n-TiO₂(001) sample and curve C is for Pt(100) surface. Same Ir-Pt tip was used for both samples. Modulation frequency of 10 kHz and modulation voltage amplitude of 10 mV peak-to-peak were employed in the phase-sensitive technique.

from the metal tip to the conduction band (i_{mc}), to the valence band (i_{mv}), and to surface states (i_{ms}) and electrons tunneling from the semiconductor to the metal tip: i_{cm} , i_{vm} , and i_{sm} . The relative magnitudes of the different components depends upon the relative locations of the Fermi levels of the metal tip and semiconductor and the location and population of surface states. When the Fermi levels are equal, no tunneling current is observed. As suggested in Scheme II, when a positive bias is applied to the tip, the Fermi

SCHEME II

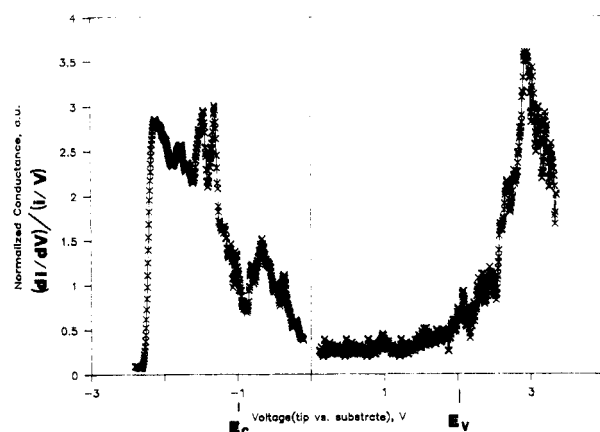
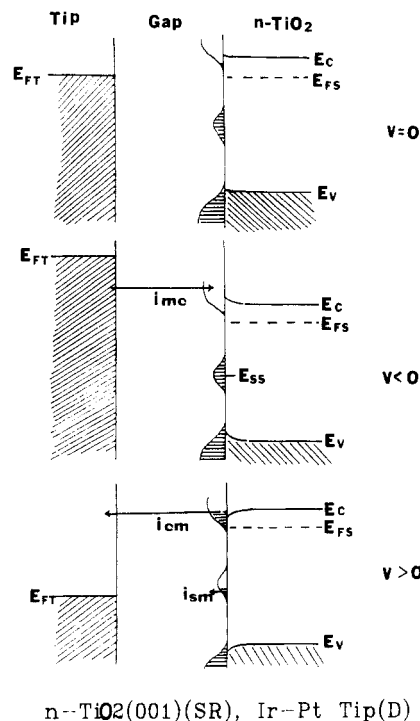


Figure 6. Ratio of dynamic to static conductance (i/V) as a function of tip voltage for an Ir-Pt tip and n-TiO₂(001) sample. Same experimental conditions as in Figure 5 were used.

level in the tip (E_{FT}) moves below that in the bulk of n-TiO₂ (E_{FS}). In the absence of surface states, as long as the Fermi energy in the tip is opposite the energy gap of the semiconductor, the tunneling current from the tip to the conduction band (CB) of the substrate (i_{mc}) will be small, because only those electrons in the tip with energies greater than the conduction band edge of n-TiO₂ will be able to tunnel to the CB of n-TiO₂. Therefore, i_{mc} decreases with increasing positive bias voltage. The second current component, flowing from the CB of the sample to the tip (i_{cm}), depends upon the tunneling probability for each state and the electron concentration at the surface of the semiconductor which will increase with increasing positive bias. We attribute the slowly increasing conductance observed in the low positively biased voltage region (e.g., <2 V) as shown in Figure 5 mainly to this current component. i_{cm} is also the major current source for the current observed at low forward bias voltage. There are two other current components, i.e., the tunneling current from the tip to the valence band (VB) of the substrate (i_{mv}) and the tunneling current from the VB of the semiconductor to the tip (i_{vm}), which are both small compared to the currents associated with the semiconductor CB at low positive bias voltage, since there are essentially no available empty states in the tip for tunneling. However, if the positive bias on the tip continues to increase (≈ 2.0 V for the present case), E_{FT} drops below the top of the VB at the

surface of the semiconductor (E_v). Now a large i_{vm} can flow, because the electrons in the VB have a large number of empty states in the tip available. We attribute the sharp increase of the conductance observed at high bias voltage (>2 V), as shown in Figures 5 and 6, to this component. However, under these bias conditions, i_{mv} will be small, since there are few empty states in the semiconductor VB.

When a negative bias is applied to the tip, i_{cm} will be small and become negligible for small negative bias, since the electron concentration at the surface of the semiconductor decreases. i_{vm} will also be small, since the electrons in the VB of n-TiO₂ see no empty states in the tip, i_{mv} will also be small in the voltage range studied, since the concentration of holes in the VB of a heavily doped wide-band-gap semiconductor is very low. i_{mc} will be small at low negative bias voltage for the present system since E_{FT} is opposite the forbidden gap in n-TiO₂. However, when the magnitude of the negative bias is increased ($\lesssim -1.0$ V for the present case) so that E_{FT} is nearly equal to the CB edge (E_c) of n-TiO₂, i_{mc} will increase very rapidly since both the surface density of states (DOS) of n-TiO₂ and the number of electrons in the tip in energy states above the conduction band edge of the semiconductor increases rapidly. The conductance spectrum shown in Figure 5 agrees with the predicted tunneling behavior quite well and suggests that conductance measurement can be used as a tool for probing the energy band edges, and hence the band gap, of semiconductors. However, the influence of the voltage drop across the semiconductor (V_s) cannot be neglected for lightly doped samples. For the heavily doped n-TiO₂ samples, e.g., with a doping density of ca. 10^{19} cm⁻³ as studied here, V_s in the conduction well region is estimated to be less than 0.1 V for most of the tip-sample separation gaps employed.

Also shown in Figure 5 are some pronounced features in the region ascribed to CB and VB energies, which might be due to oxygen p derived resonances in the VB region and titanium d derived resonance states in the CB region. However, the electronic structures of the tip could, in principle, contribute to the spectroscopic observations. To evaluate this contribution and to test the TS system used here, we carried out spectral measurements on a Pt(100) surface using the same Pt-Ir tip. A typical unnormalized conduction spectrum for the Pt(100) surface is shown in curve C of Figure 5. Note that the spectrum is quite different from that of the n-TiO₂(001) surface, showing only a broad band located at ca. 1.4 eV above the Fermi level of the Pt(100) surface. A peak at about the same energy but with a slightly broader peak width has been observed by inverse photoemission spectroscopy (IPS).¹⁸ Thus, we believe that the shapes of the spectra observed for n-TiO₂(001) surface are mainly contributed by the substrate itself.

Since di/dV increases exponentially both with voltage and with decreases in separation,^{15,19-21} these effects tend to mask smaller features that provide further details about the surface density of states. To remove these exponential dependences, one can plot the normalized conduction, i.e., the ratio of dynamic (di/dV) to static (i/V) conductance, spectra, as suggested by Feenstra et al.²² As shown in Figure 6, the normalized conductance spectrum in the positive-bias region is not very different from the unnormalized one. However, normalization considerably affects the conductance spectrum in the negative-bias region. Several well-defined peaks, which correspond well to various peaks, shoulders, and bumps observed in the unnormalized spectrum, appear. A prominent peak is seen at ca. -0.7 V, which is ca. 0.3 eV below the energy we take as the CB edge (i.e., the potential where the conductance deviates sharply from the base line). Kasowski et al.²³ predicted a state at this energy on the n-TiO₂(001) surface, on the basis of theoretically calculated one-electron density of states (DOS),

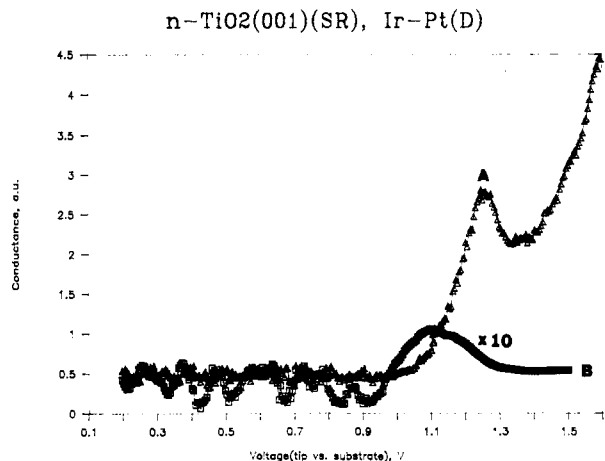


Figure 7. Dynamic (differential) conductance (A) and the ratio of dynamic to static (integral) conductance (B) as functions of bias voltage on an expanded scale for an Ir-Pt tip and n-TiO₂(001) sample. Same experimental conditions as in Figure 5 were used.

and attributed this to the lower oxygen coordination of the surface Ti atoms. We thus tentatively associate this peak with tunneling from the tip to ionized donor states. Following this peak there is a broad peak with a full width at half-maximum of ca. 1.1 eV, showing fine structure. From its location in voltage and its consistency with the theoretical calculations for the n-TiO₂(001) surface,^{23,24} we attribute this peak with tunneling from the tip into the CB of n-TiO₂.

In the positively biased voltage region, the conductance spectrum shows apparently smoothly varying behavior at low voltages starting to rise sharply at ca. 2 V, where we define the VB edge, and peaks at ca. 3 V. We attribute this broad peak to electron tunneling from the VB of n-TiO₂ to the tip (i.e., i_{vm}). To reveal more detailed structure in the low-positive-bias region, we carried out the conductance measurement on an expanded scale. As shown in Figure 7, the only feature that can be clearly identified as a peak is located at ca. 1.1 V, which is ca. 0.9 eV above the valence band edge of the n-TiO₂(001) surface. The amplitude of the peak is less than 5% of that due to the resonance states inside the valence band, suggesting that there is no appreciable low-lying oxygen p derived gap states. This is in good agreement with the UPS studies by Henrich et al.²⁵ and with the theoretical calculations for the n-TiO₂(001) surface by Munnix et al.,²³ although Tait et al.²³ have found that there is a large band of low-lying gap states for the (001) surface.

Note that although a plot of normalized conductance vs voltage provides useful information on the surface DOS of the sample and tip, the exact heights and positions of the peaks may depend on the tip-sample separation,^{26,27} the doping density and band gap of the semiconductor, and the presence of a high density of intrinsic gap states and extrinsic states due to water and other adsorbates from the air. Moreover, interpretations are probably less reliable for the voltage region where both the dynamic conductance and the current are both very small.

Conclusions

These experiments demonstrate the usefulness of the STM in conjunction with its related spectroscopic techniques for studying the n-TiO₂ surface, which is an important photocatalyst.

They show that it is possible to obtain useful information about surface and resonance electronic states and the topography of the n-TiO₂(001) surface at atomic, or near-atomic, resolution.

The STM can thus complement other techniques in studies of semiconductor surfaces, even in gases and liquids. There are fundamentally important questions concerning spatial variation

(18) Drube, R.; Dose, V.; Goldmann, A. *Surf. Sci.* **1988**, *197*, 317.

(19) Baratoff, A. *Physica B* **1984**, *127*, 143.

(20) Selloni, A.; Carnevali, P.; Tosatti, E.; Chen, C. D. *Phys. Rev. B* **1985**, *31*, 2602.

(21) Lang, N. D. *Phys. Rev. B* **1986**, *34*, 5947.

(22) Feenstra, R. M.; Stroscio, J. A.; Fein, A. P. *Surf. Sci.* **1987**, *181*, 295.

(23) Kasowski, R. V.; Tait, R. H. *Phys. Rev. B* **1979**, *20*, 5168.

(24) Munnix, S.; Schmeits, M. *Phys. Rev. B* **1984**, *30*, 2202.

(25) Henrich, V. E.; Kurtz, R. L. *Phys. Rev. B* **1981**, *23*, 6280.

(26) Chen, C. J. *J. Vac. Sci. Technol. A* **1988**, *6*, 319.

(27) Lang, N. D. *Phys. Rev. Lett.* **1986**, *56*, 1164.

of electronic structure over a surface and the association of different states with various surface defects and chemical contamination. These should be addressable by use of TS in the surface-scanning mode and are now under investigation.

Acknowledgment. The support of this research by the Office

of Naval Research and the National Science Foundation (CHE8805865) is gratefully acknowledged. We appreciate the assistance of Dr. J. Kwak in the construction of the computer interface.

Registry No. TiO₂, 13463-67-7.

Aggregation of Azo Dyes Containing Pentafluoroaniline as a Diazo Component in Aqueous Solutions

Kunihiro Hamada,*[†] Toshiro Iijima,[‡]

Department of Polymer Science, Tokyo Institute of Technology, Ookayama, Meguro-ku, Tokyo 152, Japan

and Shigetoshi Amiya

Central Research Laboratories, Kuraray Co. Ltd., Sakazu 2045, Kurashiki 710, Japan

(Received: September 29, 1989)

The aggregation of monoazo sulfonic dyes containing pentafluoroaniline as a diazo component in aqueous solutions was investigated by means of ¹⁹F NMR and electronic absorption spectroscopy. The five fluorine atoms attached to the benzene ring gave a NMR spectrum with one doublet and two triplets. With an increase in dye concentration, all the signals of the fluorines exhibited progressive shifts to lower magnetic field, indicating that the fluorine atoms in the aggregate are located outside the aromatic ring of an adjacent dye molecule. The direction of the shifts did not vary from dye to dye, but the extent did, depending on the number of sulfonic groups. The results are used to suggest a molecular model of dye aggregation. The visible absorption spectra of the dye solutions showed a single monomer/dimer equilibrium. This result permitted the calculation of aggregation constants, *K*. These *K* values agreed quite well with those determined by ¹⁹F NMR spectroscopy. The aggregation constants depended on the presence of fluorine atoms and the number of sulfonic groups. The mechanism of these effects on the aggregation is also discussed in detail.

Introduction

It is well-known that aggregated molecules behave differently from their monomers. For example, the electronic absorption spectra of dye aggregates in aqueous solutions are quite different from those of dye monomers. Recently the characteristics of aggregates such as J-aggregated dyes have been studied extensively.¹⁻⁴ The authors of these studies tried to utilize photoconductivity and intense electroluminescence of J-aggregates as a sensitizer. Cyanine dyes have also recently been investigated in the same connection.^{5,6} The aggregation behavior of azo dyes is also a matter of interest and has been widely investigated.⁷⁻¹² Imae et al. studied the micellization of a surface-active azo dye in aqueous methanol solutions in detail.^{13,14} Shimomura et al. prepared azobenzene-containing amphiphiles and investigated their aggregation behaviors in water by means of electron microscopy, differential scanning calorimetry, and absorption spectroscopy.¹⁵ As a result, it was found that the aggregate structures depended on the length of the alkyl chain in the amphiphiles and were classified into H-aggregates and J-aggregates.

We have studied the aggregation behavior of azo dyes containing one trifluoromethyl group in aqueous solutions by means of visible absorption spectra and ¹⁹F NMR measurements.¹⁶⁻¹⁸ From the chemical shifts of the fluorine atoms, an aggregate model was proposed. Blears et al.,^{19,20} Veselkov et al.,^{21,22} and Asakura et al.²³ applied ¹H NMR spectroscopy to aggregation studies, but the assignment of ¹H NMR signals is more complicated and the change in the chemical shifts of ¹H NMR is smaller than that of ¹⁹F NMR. Furthermore, ¹⁹F NMR spectroscopy is a powerful technique for the exploration of the microenvironment in the vicinity of fluorine atoms.

In the present work, monoazo sulfonic dyes containing pentafluoroaniline as a diazo component were prepared, and their

- (1) Dan, P.; Willner, I.; Dixit, N. S.; Mackey, R. A. *J. Chem. Soc., Perkin Trans. 2* **1984**, 455.
- (2) Hada, H.; Hanawa R.; Haraguchi, A.; Yonezawa, Y. *J. Phys. Chem.* **1985**, *89*, 560.
- (3) Natoli, L. M.; Ryan, M. A.; Spitzer, M. T. *J. Phys. Chem.* **1985**, *89*, 1448.
- (4) Era, M.; Hayashi, S.; Tsutsui, T.; Saito, S. *J. Chem. Soc., Chem. Commun.* **1985**, 557.
- (5) Herz, A. H. *Photogr. Sci. Eng.* **1974**, *18*, 323.
- (6) Herz, A. H. *Adv. Colloid Interface Sci.* **1977**, *8*, 237.
- (7) Pugh, D.; Giles, C. H.; Duff, D. G. *Trans. Faraday Soc.* **1971**, *67*, 563.
- (8) Duff, D. G.; Kirkwood, D. J.; Stevenson, D. M. *J. Soc. Dyers Colour.* **1977**, *93*, 303.
- (9) Datyner, A.; Floers, A. G.; Pailthorpe, M. T. *J. Colloid Interface Sci.* **1980**, *74*, 71.
- (10) Jones, F.; Kent, D. R. *Dyes Pigm.* **1980**, *1*, 39.
- (11) Reeves, R. L.; Maggio, M. S.; Harkaway, S. A. *J. Phys. Chem.* **1979**, *83*, 2359.
- (12) Takagishi, T.; Fujii, S.; Kuroki, N. *J. Colloid Interface Sci.* **1983**, *94*, 114.
- (13) Imae, T.; Mori, C.; Ikeda, S. *J. Chem. Soc., Faraday Trans. 1* **1982**, *78*, 1359.
- (14) Imae, T.; Mori, C.; Ikeda, S. *J. Chem. Soc., Faraday Trans. 1* **1982**, *78*, 1369.
- (15) Shimomura, M.; Ando, R.; Kunitake, T. *Ber. Bunsen-Ges. Phys. Chem.* **1983**, *87*, 1134.
- (16) Hamada, K.; Kubota, H.; Ichimura, A.; Iijima, T.; Amiya, S. *Ber. Bunsen-Ges. Phys. Chem.* **1985**, *89*, 859.
- (17) Hamada, K.; Take, S.; Iijima, T.; Amiya, S. *J. Chem. Soc., Faraday Trans. 1* **1986**, *82*, 3141.
- (18) Skrabal, P.; Bangerter, F.; Hamada, K.; Iijima, T. *Dyes Pigm.* **1987**, *8*, 371.
- (19) Blears, D. J.; Danyluk, S. S. *J. Am. Chem. Soc.* **1966**, *88*, 1084.
- (20) Blears, D. J.; Danyluk, S. S. *J. Am. Chem. Soc.* **1967**, *89*, 21.
- (21) Veselkov, A. N.; Dymant, L. N.; Kulikov, E. L. *Khim. Fiz.* **1984**, *3*, 1108.
- (22) Veselkov, A. N.; Dymant, L. N.; Kulikov, E. L. *Zh. Struct. Khim.* **1985**, *26*, 43.

* Present address: Faculty of Textile Science and Technology, Shinshu University, Ueda-shi, Nagano 386, Japan.

† Present address: Jissen Women's University, Hino-shi, Tokyo 191, Japan